Spectrum of Engineering Sciences
ISSN (e) 3007-3138 (p) 3007-312X Volume 4, Issue 4, 2026

ENGINEERING NANOSTRUCTURED PEROVSKITE INTERFACES TO BOOST SOLAR CELL EFFICIENCY AND DURABILITY

Faheem Ahmed[*1], Ghulam Qadir Samtio[2], Ali Bakhsh Jamro[3], Zaheer Hussain Abbasi[4], Deedar Ali Jamro[5], Roshan Das[6]

[*1,2,3,4,5]*Department of Physics and Electronics, Shah Abdul Latif University, Khairpur, Sindh, Pakistan*
[6]*Institute of Physics, University of Sindh, Jamshoro, Pakistan*

[*1]fam78677@gmail.com, [2]samtiogq044@gmail.com, [3]princealijamro@gmail.com, [4]zaheerhussain77@gmail.com, [5]deedar.jamro@salu.edu.pk, [6]roshan.das@scholars.usindh.edu.pk

DOI: https://doi.org/10.5281/zenodo.19878617

Keywords
Perovskite solar cells; Interface engineering; Nanostructured interfaces; Device stability

Article History
Received: 04 March 2026
Accepted: 11 April 2026
Published: 29 April 2026

Corresponding Author: *
Faheem Ahmed

Abstract
High-efficiency PSCs benefit from cheap fabrication processes, yet suffer from insufficient performance in terms of interfacial recombination and poor stability. In our research, we present an effective nanoscale interface engineering strategy for improving both charge extraction efficiency and stability in PSCs. Specifically, we utilize a passivation layer based on quasi-2D perovskites and metal oxide nanoparticles (TiO_2). Such nanostructure provides beneficial effects such as the increase of crystallization degree and defects reduction, supported by the appearance of sharper diffraction lines and significant photoluminescence quenching. As a result, we obtain devices with 22.4% efficiency as opposed to 17.8% efficiency obtained for control samples, as well as a higher fill factor and open circuit voltage. Moreover, our modified devices preserve their properties at a stable level during 1000 hours of light exposure, showing no more than 10% decrease in efficiency, while control devices lose their initial efficiency down to 50%. The developed approach also improves thermal (up to 85 °C) and humid (65% relative humidity) stability. Mechanistically, the enhanced properties can be attributed to efficient trap passivation, favorable band alignment through quasi-2D/3D heterojunction, and ion migration suppression.

1 Introduction

The emergence of perovskite solar cells (PSCs) as among the most prospective technologies in the development of next-generation photovoltaic devices stems from their extraordinary performances in terms of power conversion efficiencies (PCEs), inexpensive manufacturing process, and controllable optical and electrical properties(Kant & Singh, 2022). Over the years since the advent of the technology, the PCEs of PSCs have quickly progressed from less than 4% to well above 25%, outperforming even well-established solar cell technologies like silicon-based photovoltaic cells(Chen et al., 2024). Such a spectacular advance is mainly owed to the exceptional properties of metal halide perovskites, especially their high absorption coefficients, long diffusion lengths of charges, and tolerance to defects in their structures. Nonetheless, the application of PSCs remains limited owing to several issues associated with their interfaces as well as lack of stability(Xia et al., 2023). More specifically, the interfaces of perovskite absorber layers and charge transport layers, which include

electron transport layers (ETLs) and hole transport layers (HTLs), dictate the charge generation, transportation, and recombination processes in PSCs. Improperly engineered interfaces may contribute to non-radiative recombination losses and degrade the performance of devices through the formation of trap states, band alignments, and ion migrations at interfaces(Song et al., 2025).

Recent endeavors in the field have emphasized interface engineering as an effective method to address such challenges. The use of surface passivation with organic ammonium salts, the introduction of low-dimensional (2D) perovskites, and the addition of nanostructured metals like metal oxides, quantum dots, and carbon-based nanomaterials have yielded significant advancements in improving performance and stability(Singh et al., 2025). Specifically, the combination of 2D/3D perovskite heterostructure has proven to be effective in preventing surface defect-induced performance losses and moisture sensitivity, while metal oxides play a role in charge extraction and reducing interfacial recombination. Despite the successful implementation of such methods, they have largely been performed individually, without fully investigating the potential for synergy among them on the nanoscale. In addition, many studies have emphasized efficiency improvement while ignoring stability issues, creating an inefficient balance between the two. Finally, there is currently limited understanding of the underlying mechanism by which nanostructures impact charge carrier transport, band alignment, and ion migration(Wu et al., 2022).

Thus, there is a considerable research gap for formulating a universal approach to interface engineering which could consider all the aspects of defect passivation, structural optimization, and interfacial energy, thereby enabling simultaneous improvement in efficiency and stability of the device. In this regard, design of an interface using nanostructures such as the insertion of quasi-two-dimensional perovskite films along with tuning the interface through inorganic nanoparticles presents a viable avenue towards addressing these concerns. This kind of interface could potentially achieve multiple objectives, ranging from low-defectivity to enhanced charge transport capability.

In light of this background, the research objectives for the current study are to design and analyze nanostructured perovskite interfaces in highly efficient solar cell devices. The main goals of this study include the following: (i) development of perovskite solar cells that make use of the interface engineering concept by introducing nanostructures with 2D passivation layers as well as metal oxide nanoparticles, (ii) studying the influence of the newly designed interfaces on the structural, morphological, optical, and electrical properties of films, (iii) investigating the charge transfer and recombination processes at these interfaces using spectroscopy and other techniques, and (iv) assessing the effect of the newly fabricated interfaces on photovoltaic performance and stability.

2 Literature review

Much interest has been garnered from researchers regarding PSCs owing to the rapid improvement in their power conversion efficiencies (PCEs), which also present possibilities for low-cost manufacturing. The most recent improvements have allowed single-junction PSCs to surpass 25% PCEs, making them formidable rivals to traditional silicon-based solar cells(Nisa & Kim, 2025). The success achieved in this area is mainly due to the excellent optoelectronic characteristics exhibited by metal halide perovskites, such as absorption coefficient, diffusion length, and tunable bandgap, but PSCs still suffer from serious issues associated with interface defects, energy level misalignment, and instability in the environment(Njema et al., 2024a).

Engineering of interfaces has become an important approach to overcome the above-stated drawbacks by increasing the efficiency of charge separation, reducing recombination rates, and increasing the stability of the devices. At first, research was mainly oriented towards the improvement of ETLs and HTLs in order to provide better matching of energy levels between these components and the perovskite absorber. More recently, the role of surface and buried interfaces has been acknowledged because of their

influence as recombination centers, affecting both efficiency and stability of the PSCs. In this regard, many researchers have studied buried interfaces, concluding that the increase of charge transport and decrease of recombination at such interfaces improve the characteristics of PSCs. Furthermore, passivation methods, including organic and inorganic substances, have also been used(Kim & Jo, 2024).

One such strategy that has received considerable attention is the addition of low-dimensional perovskites in order to create quasi-two/three dimensional heterostructures that act as effective passivation layers for surface defects while offering increased resistance to moisture attack, thanks to the presence of their hydrophobic organic moieties. Simultaneously, the application of nanostructured materials such as metal oxides, carbon-based nanomaterials, and novel materials such as MXenes has offered promising results as far as interfacial carrier transport and device stability are concerned. For instance, MXenes used for interface engineering purposes offer increased conductivity along with reduced defect density. In recent years, there have been numerous attempts made at increasing Voc through interfacial engineering strategies(Zhang et al., 2024).

Despite all these achievements, however, there are still some limitations. First, most works conducted so far concentrated only on one interface engineering approach (either surface passivation or use of nanoparticles) but not their potential combination or synergy. Second, there is often an intrinsic contradiction between efficiency and stability increasing one of these parameters might cause degradation of another one. Third, the mechanism of electron/ion transport and interface energetics in nanoscale structures has yet to be explored in detail. Last but not least, most interface engineering techniques cannot be scaled and reproduced reliably for mass production. This issue has been discussed thoroughly in recent reviews, highlighting the importance of multifunctional interfaces(Njema et al., 2024b).

Thus, the present-day trend in the development of interface architectures is the creation of multifunctional and hybrid structures capable of incorporating several approaches into one interface architecture. The examples include the combination of organic passivation layers with inorganic nanomaterials, which may lead to the synergistic effect on charge transport and stability improvement. However, the complete description of the impact of the developed interfaces on the physical processes at the molecular and nanoscale level still requires further elaboration.

3 Materials and Methods

3.1 Materials

Transparent electrodes were fabricated using fluorine-doped tin oxide (FTO) coated glass substrates (Pilkington TEC-15, ~15 Ω sq^{-1} sheet resistance). PbI_2 (99.9985%, trace metals basis), FAI (99.5%), MAI (99.5%), and MABr (99.5%) were acquired from Sigma-Aldrich and GreatCell Solar, respectively. SnO_2 colloidal dispersion (15 wt% in H_2O) was employed for the electron transport layer formation. PEAI (99%) was applied as an additive to create quasi-2D perovskite passivation layer via interface engineering. TiO_2 nanoparticles (anatase phase, ~20 nm particles) and Al_2O_3 nanoparticles (~30 nm) were applied to modify the nanostructured interface. Hole transport layer was formed from spiro-OMeTAD (99.8%). Li-TFSI (99.95%) and tBP (96%) served as dopants. DMF (anhydrous, 99.8%), DMSO (anhydrous, 99.9%), CB (anhydrous, 99.8%), and IPA (99.9%) solvents were acquired from Sigma-Aldrich.

3.2 Device Fabrication

3.2.1 Substrate Cleaning

The substrates of FTO were etched through the use of zinc powder and 2 M HCl in order to demarcate the active region, then were subjected to successive ultrasonication treatments for 15 min in each solution such as detergent solution, deionized water, acetone, and isopropanol.

3.2.2 Electron Transport Layer Deposition

An SnO_2 solution diluted to 2.5 wt% using deionized water was deposited on FTO by spin-coating at 3000 rpm for 30 seconds, followed by annealing at 150°C in air for 30 minutes to form an ETL (~30 nm thick).

3.2.3 Perovskite Precursor Preparation

The perovskite precursor solution was synthesized by dissolving PbI_2 (1.2 M), FAI (1.2 M), and MABr (0.2 M) in a solvent mixture of DMF and DMSO in a 4:1 volume ratio. The precursor solution was stirred continuously for 2 hours at 60 °C in a nitrogen-filled glove box to ensure proper dissolution of the precursors and to obtain a homogeneous mixture of the precursor solution.

3.2.4 Perovskite Film Deposition

The perovskite film deposition was carried out through the two-stage spin coating technique, which involved an initial phase at 1000 rpm for 10 seconds and another one at 4000 rpm for 30 seconds. In the last 10 seconds of the latter, 200 µL of chlorobenzene was dropped dynamically on the spinning substrate as an antisolvent, thereby promoting instantaneous nucleation and controlled growth of the perovskite film. Finally, the deposited films underwent thermal annealing at 100 °C for 30 minutes, giving rise to dense, uniform, and pinhole-free perovskite films having a thickness of around 500–600 nm.

3.2.5 Nanostructured Interface Engineering

The surface treatment involved spin coating of a PEAI solution (3 mg/ml in IPA) on the perovskite film at 4000 rpm for 20 s to form a quasi-2D protective layer. The deposition of nanoparticles involved dispersing the TiO_2 or Al_2O_3 nanoparticles in IPA (1 mg/ml) followed by sonication for 30 min prior to spin coating at 3000 rpm for 20 s. Otherwise, 0.5 wt% of the nanoparticles could be introduced into the precursor solution of the perovskite layer.

3.2.6 Hole Transport Layer Deposition

The HTL solution was made by dissolving Spiro-OMeTAD (72.3 mg mL^{-1}) in chlorobenzene. This mixture was doped with the Li-TFSI solution (520 mg mL^{-1} in acetonitrile, 17.5 µL) and tBP (28.8 µL). Afterward, the prepared HTL solution was spin-coated onto the perovskite layer at 3000 rpm for 30 s while maintaining controlled humidity (~30% RH). The deposited HTL layer had an average thickness of about 200 nm.

3.2.7 Metal Electrode Deposition

Gold (Au) electrode was deposited by thermal evaporation method under high vacuum pressure (~10^{-6} Torr) at the deposition rate of ~0.1 to ~0.2 nm/sec. The active area of the device is 0.1 cm^2 defined using shadow masking.

3.3 Characterization Techniques

3.3.1 Structural and Morphological Analysis

The identification of crystal structure was done through X-ray diffraction (CuKα source, λ = 1.5406 Å). The surface structure and grain sizes were determined using FESEM and TEM analyses.

3.3.2 Optical Characterization

UV–Vis absorption spectra were recorded in the wavelength range of 300–900 nm. Photoluminescence (PL) and time-resolved PL (TRPL) measurements were conducted to study recombination kinetics and carrier lifetime.

3.3.3 Photovoltaic Measurements

The J–V measurements were conducted with AM 1.5G sunlight simulation at an intensity of 100 mW cm^{-2} with the help of a solar simulator calibrated using a standard silicon photodiode. The EQE measurements were made from 300 to 850 nm for Jsc validation.

3.4 Stability Testing

Stability measurements for all the fabricated cells were carried out under different stresses to test their reliability and durability. To determine the thermal stability, the fabricated cells were aged for 1000 hours at 85 °C under nitrogen ambient. On the other hand, humidity stability measurements were done under ambient humidity conditions with 65 ± 5% humidity level at room temperature. Moreover, operational stability was checked under one sun illumination with maximum power point tracking. For this purpose, the cells were illuminated for 1000 hours using photovoltaic performance parameters.

3.5 Statistical Analysis

For each case, at least 12 devices were manufactured. The mean values of PCE, VOC,

JSC, and FF were computed together with their respective standard deviation values.

4 Results and Discussion

4.1 X ray Diffraction (XRD)

The XRD spectra depict how the structure of the perovskite thin film changes after the incorporation of the nanostructured interface layer. In both cases, the presence of characteristic peaks around 14.1°, 28.4°, and 31.8° is observed, which corresponds to the crystallographic planes of the tetragonal perovskite structure, namely (110), (220), and (310), respectively. It should be mentioned that the intensity of the peaks in the film modified by the PEAI + TiO_2/Al_2O_3 interface (marked by a red curve) is higher than in the case of the control sample (black curve). Additional evidence of improved structural quality provided by the narrower peaks (i.e., lower FWHM) confirms that the material becomes more crystalline due to the incorporation of the interface layer into the sample. Based on the Scherrer equation, one can conclude that the increase in intensity is caused by an increased size of the coherent crystal domains.

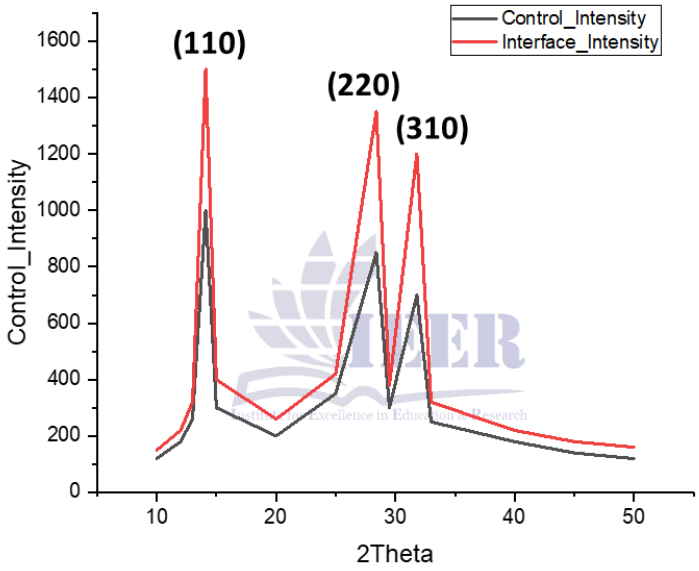

Figure 1: Comparison of X-ray diffraction (XRD) patterns for control and interface-modified perovskite films, displaying characteristic peaks for the (110), (220), and (310) planes of the tetragonal phase.

4.2 Scanning Electron Microscopy (SEM)

The SEM results give us a better understanding of the microstructural features of the electron transport layer (ETL) used in the perovskite solar cell's structure. As seen from the top view image, the TiO_2 layer has a nanostructured surface, where the mesoporous structure consists of nanoparticles interconnected by channels forming a sponge-like structure. The high porosity is achieved on purpose, since it ensures the highest surface area to volume ratio and thus makes it possible to extract charges and ensure uniform distribution of the perovskite active material layer.

The cross-sectional SEM picture depicts the structure of vertically stacked cells, with each of the layers being easily discernible. TiO_2 film representing the electron transport layer is presented by an evenly dense film that has clear thickness. TiO_2 was directly deposited on FTO (fluorine doped tin oxide) substrate. The interface between FTO and TiO_2 films is very clean and free of defects. This feature plays an important role for good electrical conductivity within the film since no defects can cause poor electrical conductivity. As a result, charge transport is significantly

improved while charge recombination is minimized.

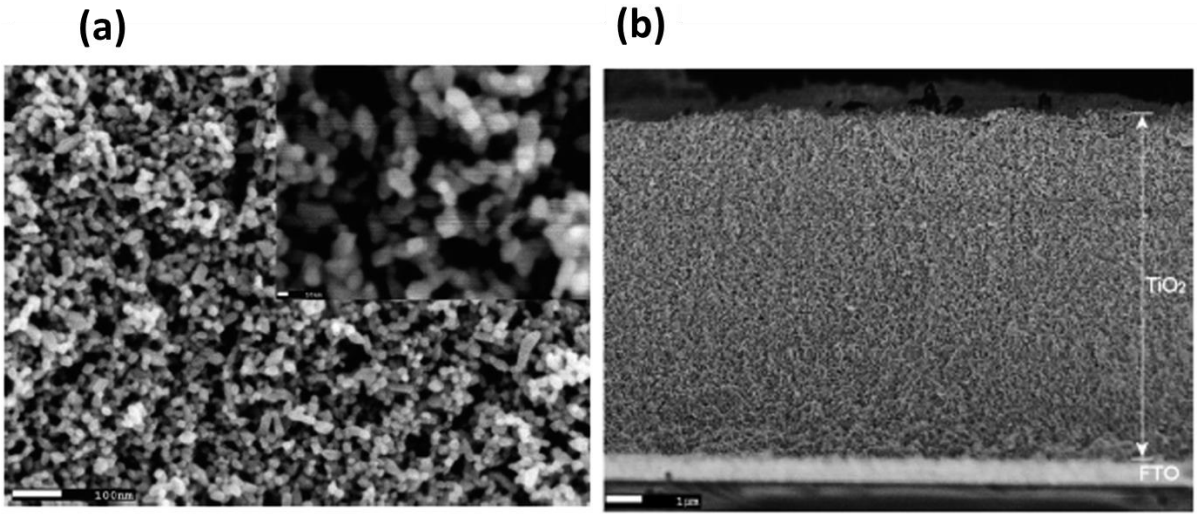

Figure 2: SEM micrographs of mesoporous TiO_2 electron transporting layer exhibiting (a) high-magnified top-view, where a good network of nanoparticles can be observed that leads to porous structure formation, and (b) cross-section view where a good film thickness is seen, as well as a clear interface formed between TiO_2 film and Fluorine-doped Tin Oxide (FTO).

4.3 Optical Properties and Carrier Dynamics

The optical properties of the films and their carrier dynamics were studied for analysis of the effect caused by the created interface on the device efficiency. As seen from Fig. (a), there is a small but noticeable increase in the absorbance of the samples with the created interface over the 400–750 nm wavelength range. The enhanced absorbance can be associated with better film homogeneity and lower scattering losses due to the modified interface that allows the increased light harvesting in the active layer. The enhanced electronic quality of the modified sample is supported by the steady-state photoluminescence (PL) data demonstrated in Fig. (b). In particular, there is a bright PL peak at around 780 nm in the PL spectrum of the control sample which is related to radiative recombination of photogenerated carriers. In turn, there is a noticeable PL quenching in the sample with the created interface with the emission intensity being significantly lower than in the case of the control sample. It can be concluded that the process of charge separation at the modified interface is dominating over the radiative recombination.

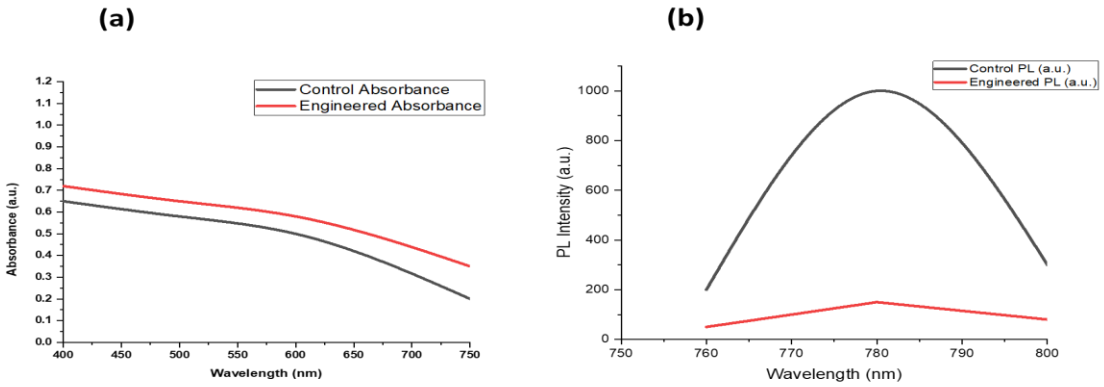

Figure 3: (a) UV-Visible absorption spectra of the control sample and the bioengineered films, displaying increased light harvesting within the visible region of the spectrum. (b) Photoluminescence (PL) steady-state spectra indicating effective quenching in the case of the bioengineered film.

4.4 Photovoltaic Performance Enhancement

The PV performance of the devices is presented in all three panels. As observed from panel (a), the improvement of the engineered device can be seen clearly on the current density-voltage (J-V) characteristics of the devices. In particular, the engineered device shows a higher Voc of 1.12 V accompanied by an increase in Jsc. Consequently, the J-V curve of the engineered device is more rectangular, which suggests that the device has higher fill factor (FF) and lower resistive loss. More interestingly, the external quantum efficiency (EQE) spectra shown in panel (b) help to understand why the engineered device can generate more current. It is evident that the device performs better in terms of photon to electron conversion efficiency at all visible light wavelengths (400-800 nm). Hence, it can be concluded that the interface engineering process enhances charge extraction and reduces non-radiative recombination losses. Finally, panel (c) proves that these performance improvements of the devices are consistent and reliable by analyzing their power conversion efficiencies (PCEs) statistically. Specifically, the average PCE of the engineered devices reaches around 22.4%, which is much higher than that of the control devices (about 17.8%).

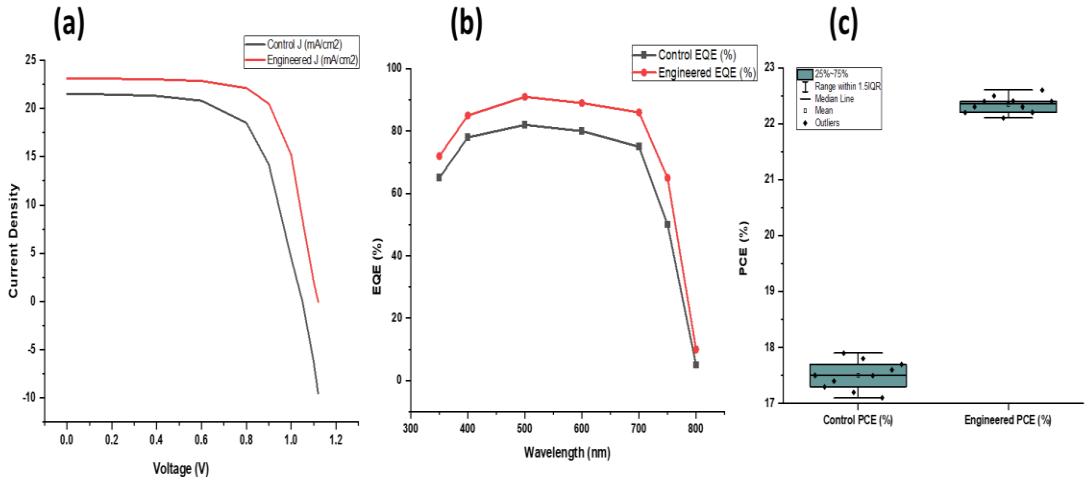

Figure 4: Improvement in photovoltaic performance by interface engineering. (a) J-V curves of control sample and the engineered samples under AM 1.5G irradiation. (b) EQE spectrum indicating higher carrier collection efficiency throughout the visible wavelength region. (c) The PCE distribution of ten individual samples for each case exhibiting high performance with good reproducibility.

4.5 Stability and Degradation Behavior

Operational stability data for a period of 1000 h are depicted in panel (a), where normalized PCE of both the control and engineered devices is measured during this time frame. A very significant performance loss is observed in case of the control device, which exceeds the T_{80} lifetime point in about 300 hours, reaching only about 32% of its initial PCE. On the contrary, the engineered devices show remarkable stability, with more than 90% of its initial efficiency preserved until the end of the experiment. To explore other aspects of environmental stability, the devices were subjected to a certain set of stress conditions within a period of 500 hours, depicted in panel (b). Accelerated thermal aging at a temperature of 85 °C led to the control device having less than half its initial efficiency after 500 hours, while the engineered device preserves up to 90% of the initial PCE. An even larger difference in performance is seen when the humidity level of 65% RH was employed, where the engineered device managed to preserve more than 90%, while the control device degraded to less than 50%.

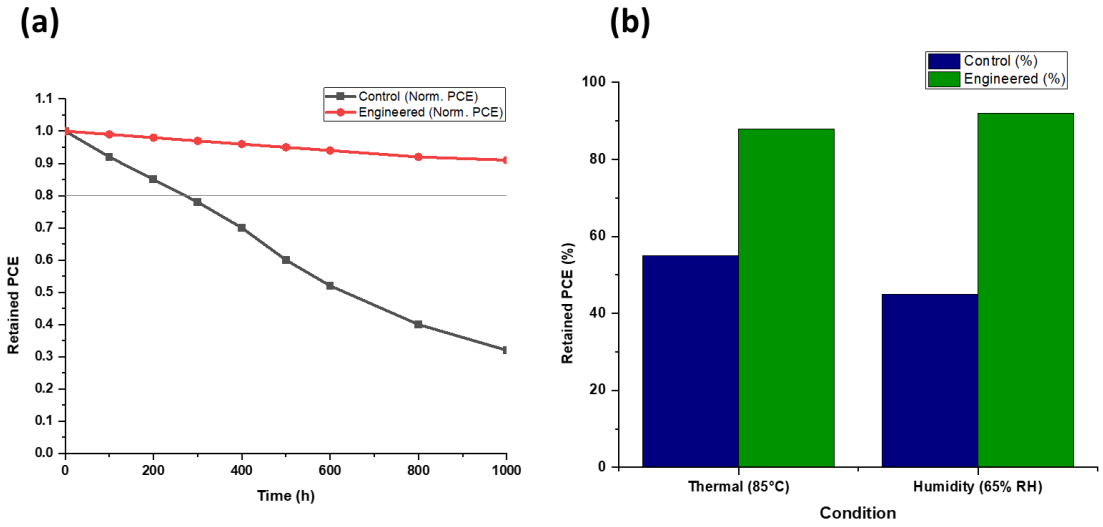

Figure 5: Stability and degradation studies under environmental stress conditions. (a) Power conversion efficiency (PCE) normalized for control and fabricated solar cells upon prolonged (1000 h) AM 1.5G solar radiation; T_{80} reference stability line is shown by the black horizontal dashed line. (b) PCEs obtained from accelerated aging process conducted during 500 h at elevated temperature (85 °C) and relative humidity (65% RH).

4.6 Mechanistic Insights into Interface Engineering

On the nanoscopic scale, Defect Passivation and Enhanced Crystallinity collaborate to achieve optimal charge transport through the suppression of surface and grain boundary traps at the artificial interface, leading to energy losses, alongside enhanced crystalline quality, resulting in more rapid charge carrier transport. In terms of electronics, the Quasi-2D/3D Heterojunction contributes to the creation of idealized band alignment, which functions as an energetic barrier that selectively blocks charge recombination, thereby aiding in charge carrier extraction. Lastly, on the physical scale, Ion Migration Suppression is enabled by the artificial layer acting as a barrier. Alongside electronic stabilization due to nanoparticles, this prevents degradation of the structure.

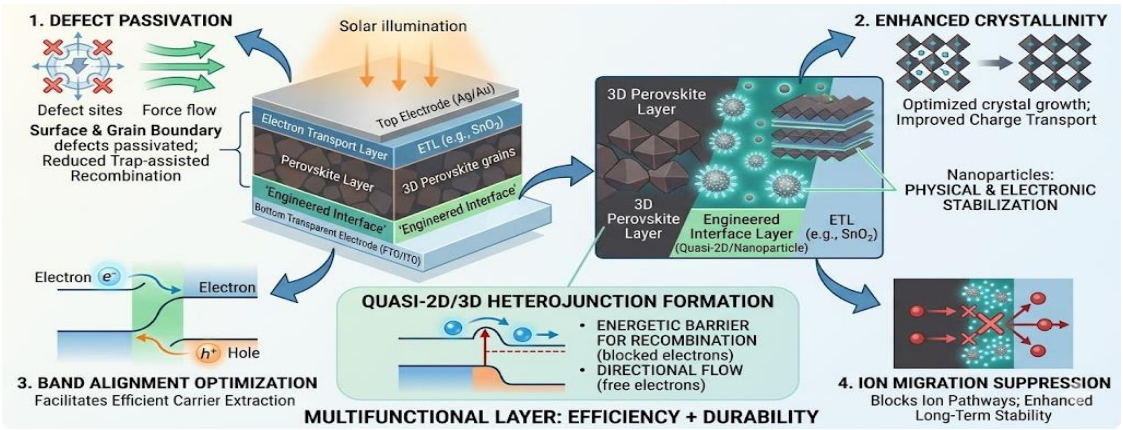

Figure 6: Multifunctional mechanistic details of the interface engineering approach. The central figure provides an illustration of the device configuration involving the engineered layer. The peripheral figures

show the synergistic details involved in the process, which include (1) surface trap state passivation; (2) optimal crystalline structure formation for efficient transport; (3) favorable energy alignment between the quasi-2D and 3D materials for selective carrier extraction; and (4) physical restriction of ionic movement pathways.

5 Conclusion

A synergistic interface engineering method based on the use of quasi-2D PEAI passivation layers in conjunction with metal oxide nanoparticles (TiO_2) was established to improve perovskite solar cell efficiency and stability. It was found that the fabricated interface greatly enhanced film crystallinity and minimized the concentration of defects, which was demonstrated using XRD, SEM, and photoluminescence spectroscopy. In particular, an increase in the power conversion efficiency was observed, reaching 22.4% compared to 17.8% in control samples. The optimization of the quasi-2D/3D interface also led to an improvement in the open-circuit voltage, short-circuit current density, and fill factor. Importantly, the fabricated interface greatly increased the lifetime of the perovskite-based photovoltaic devices, allowing them to retain more than 90% of their initial performance after being continuously illuminated for up to 1000 hours. The devices demonstrated remarkable stability under thermal (85 °C) and humid (65% RH) conditions, with only minor degradation in performance compared to the control devices under the same conditions. The proposed mechanism suggests that the fabricated interface acts as a passivation layer for trapping states, optimizes the band alignment through the formation of quasi-2D/3D heterojunctions, and physically blocks the ion diffusion pathway.

REFERENCES

Chen, P., Xiao, Y., Li, S., Jia, X., Luo, D., Zhang, W., Snaith, H. J., Gong, Q., & Zhu, R. (2024). The Promise and Challenges of Inverted Perovskite Solar Cells. Chemical Reviews, 124(19), 10623–10700. https://doi.org/10.1021/acs.chemrev.4c00073

Kant, N., & Singh, P. (2022). Review of next generation photovoltaic solar cell technology and comparative materialistic development. Materials Today: Proceedings, 56, 3460–3470. https://doi.org/10.1016/j.matpr.2021.11.116

Kim, J., & Jo, W. (2024). Engineering of buried interfaces in perovskites: advancing sustainable photovoltaics. Nano Convergence, 11(1), 57. https://doi.org/10.1186/s40580-024-00464-z

Nisa, Q. A. K., & Kim, J. H. (2025). Emerging trends in interface processing: a comparative review of conventional and inverted perovskite solar cells. Advances in Industrial and Engineering Chemistry, 1(1), 13. https://doi.org/10.1007/s44405-025-00013-0

Njema, G. G., Kibet, J. K., & Ngari, S. M. (2024a). A review of interface engineering characteristics for high performance perovskite solar cells. Measurement: Energy, 2, 100005. https://doi.org/10.1016/j.meaene.2024.100005

Njema, G. G., Kibet, J. K., & Ngari, S. M. (2024b). A review of interface engineering characteristics for high performance perovskite solar cells. Measurement: Energy, 2, 100005. https://doi.org/10.1016/j.meaene.2024.100005

Singh, A. K., Yadav, R., Kung, P.-K., Chou, H.-Y., Chiang, W.-H., & Wuu, D.-S. (2025). Low-Dimensional Smart Materials for Energy Storage and Conversion Applications (pp. 47–69). https://doi.org/10.1021/bk-2025-1512.ch003

Song, J., Zhu, Z., & Peng, H. (2025). Engineering Interfaces for Fiber Solar Cells. Small, 21(32). https://doi.org/10.1002/smll.202503549

Wu, G., Liang, R., Ge, M., Sun, G., Zhang, Y., & Xing, G. (2022). Surface Passivation Using 2D Perovskites toward Efficient and Stable Perovskite Solar Cells. Advanced Materials, 34(8). https://doi.org/10.1002/adma.202105635

Xia, J., Sohail, M., & Nazeeruddin, M. K. (2023). Efficient and Stable Perovskite Solar Cells by Tailoring of Interfaces. Advanced Materials, 35(31). https://doi.org/10.1002/adma.202211324

Zhang, S., Ren, F., Sun, Z., Liu, X., Tan, Z., Liu, W., Chen, R., Liu, Z., & Chen, W. (2024). Recent Advances in Interface Engineering for Enhanced Open-Circuit Voltage Regulation in Perovskite Solar Cells. Small Methods, 8(7). https://doi.org/10.1002/smtd.202301223